Observationally Constrained Cloud Phase unmasks Orbitally Driven Climate Feedbacks

N. Sagoo[1,†], T. Storelvmo[1,‡], L. Hahn[1,§], I. Tan[1±], James Danco[2,#], Bryan Raney[2], A.J. Broccoli[2]

[1]Geology & Geophysics Department, Yale University, New Haven, CT 06511, USA

[2]Department of Environmental Sciences, Rutgers, The State University of New Jersey, New Brunswick, NJ 08901, USA

[†]Department of Meteorology, University of Stockholm, 10691 Stockholm, Sweden

[‡]Department of Geosciences, P.O. Box 1047 Blindern, 0316 Oslo, Norway

[§]Department of Atmospheric Sciences, University of Washington, Seattle, WA 98195, USA

[±±]Department of Atmospheric and Oceanic Sciences, McGill University, H3A 0B9, Canada

[#]National Oceanic and Atmospheric Administration, National Weather Service, Raleigh, NC 27606, USA

Corresponding author: first and last name (navjit.sagoo@misu.su.se)

Key Points:

- Low cloud phase feedback is less negative in response to orbital forcing when cloud phase is observationally constrained by satellite data
- Shortwave cloud and net water vapor feedbacks are identified as mechanisms which amplify orbitally driven changes in insolation
- Improving cloud phase representation in models is important for understanding the climate system response to forcing in past climates

Abstract

The mechanisms which amplify orbitally driven changes in insolation and drive the glacial cycles of the past 2.6 million years, the Pleistocene, are poorly understood. Previous studies indicate that cloud phase feedbacks oppose ice sheet initiation when orbital configuration supports ice sheet growth. Cloud phase was observationally constrained in a recent study and provides evidence for a weaker negative cloud feedback in response to carbon dioxide doubling. We observationally constrain cloud phase in the Community Earth System Model and explore how changes in orbital configuration impact the climate response. Constraining cloud phase weakens the negative high latitude cloud phase feedback and unmasks positive water vapor and cloud feedbacks (amount and optical depth) that extend cooling to lower latitudes. Snowfall accumulation and ablation metrics also support ice sheet expansion as seen in proxy records. This indicates that well known cloud and water vapor feedbacks are the mechanisms amplifying orbital climate forcing.

Plain Language Summary

The recent ice ages represent large transitions in climate that are forced by small changes in solar radiation, driven by variations in the Earth's orbit. This study aims to identify plausible mechanisms that can amplify this small solar signal and lead to the development of large ice sheets, thereby improving our understanding of the climate system. Cloud phase (the proportion of liquid to ice) is poorly represented in climate models and previous work has shown that this can lead to an underestimation of the climate response to carbon dioxide forcing. This study explores the climate response to orbital forcing when cloud phase is observationally constrained by satellite. Previous modeling studies have found that when high latitude solar radiation is

reduced due to orbital variations, clouds thin, allowing more absorption of solar radiation which effectively opposes the orbital cooling that encourages ice sheet growth. We find that when cloud phase is constrained, this opposing cloud thinning is reduced and cooling extends to lower latitudes via cloud and water vapor feedbacks. Our work indicates that well understood climate processes are the mechanisms that amplify orbital climate forcing, and reiterate the importance in properly simulating cloud phase in climate models.

1. Introduction

The Earth has experienced dramatic shifts in climate from glacial to interglacial states during the Pleistocene (the past 2.6 million years). These changes are paced by changes in orbital configuration (Hays et al., 1976) but there is no satisfactory theory to fully explain how changes in orbit (eccentricity, obliquity and precession) drive ice sheet growth and decay. Obliquity refers to the angle of the Earth's axis with respect to the orbital plane with a periodicity of 41 kyr, eccentricity is the shape of the Earth's orbit from nearly circular to elliptical with a periodicity of 100 kyr, while precession, with a periodicity of 26 kyr is the 'wobble' of the Earth on its axis analogous to the wobble of a spinning top. Milutin Milanković, whose orbital theory is the leading theory, postulated that changes in Earth's orbit affecting summertime insolation were important in determining global ice volume, and that changes in orbit that led to cooler summers would increase snow and ice preservation (Milanković, 1941).

Sedimentary archives from deep sea, bottom dwelling foraminifera, record strong obliquity and precession forcing over the Cenozoic era (past 65 My) with the obliquity signal dominating these records (Lisiecki & Raymo, 2005; Raymo et al., 2006; Zachos et al., 2001; Westerhold et al., 2020). These proxies show that Pleistocene glacial climates initially varied

with a periodicity of around 40 kyr switching to 100 kyr around 1 million years ago. The precession signal is modulated by eccentricity, and is weaker in the early Pleistocene and stronger in late Pleistocene records (Huybers, 2011; Liautaud et al., 2020). Numerous hypotheses have been proposed to explain the weak precession signal in the early Pleistocene proxies, e.g. interhemispheric cancellation of ice-volume changes (Raymo et al., 2006), summer duration and intensity being anti-phased (Huybers, 2006) and meridional insolation gradients (Raymo & Nisancioglu, 2003). A recent study using statistical methods argues that precession has a stronger contribution than previously recognized in the early Pleistocene and increases through this epoch (Liautaud et al., 2020).

Whilst precession controls the intensity of summer insolation (Huybers, 2006) glaciers are sensitive to insolation integrated over the duration of the summer of which obliquity is a primary control. Our study focuses on the role of obliquity in driving the glacial climates because this is the dominant signal recorded in proxies, particularly in the early Pleistocene (Zachos et al., 2001). When Earth's obliquity is low, summers are cooler and winters are warmer, with the cool summers thought to favour the preservation of ice and glacial conditions. Changes in obliquity affect the annual mean meridional gradient in insolation with larger changes in the high latitudes than in the low latitudes. For the range of high and low obliquity values used in this work (see methods) and previous studies (Erb et al., 2013; Mantsis et al., 2011) a reduction in the obliquity from 24.480° to 22.079° leads to a reduction in high latitude insolation of up to 50 Wm^{-2} over the summer (see Figure 1). Whilst these changes in insolation are large, they are not sufficient to completely drive the glacial cycles of the Pleistocene (Rind et al., 1989; Saltzman et al., 1984; Lisiecki, 2010; Huybers, 2011; Erb et al., 2013; Mantsis et al., 2011).

The relationship among the different orbital frequencies, as well as CO_2 and dust which covary with the Pleistocene glacial cycles is complex (Martínez-Garcia et al., 2011; Petit et al., 1990; Sigman & Boyle, 2000). General Circulation Models (GCMs) which have incorporated orbital changes and additional climate forcings such as CO_2 (Barnola et al., 1987), dust (Lambert et al., 2008), vegetation (Tabor et al., 2015), topography or coupled ice sheet models (Abe-Ouchi et al., 2013) and including regolith, as previously hypothesized and tested (Clark & Pollard, 1998; Tabor & Poulsen, 2016) have had modest success in both simulating glacial inception and / or glacial melt as well as the sawtooth shape and periodicity of the glacial cycles.

Transient simulations run over several glacial cycles using Earth system Models of Intermediate Complexity (EMICs) have had considerably more success in simulating glacial-interglacial climates. Ganopolski & Brovkin, (2017) were able to simulate the temporal dynamics of CO_2 and global ice volume over the past 4 glacial cycles using orbital variability as the only external forcing. The timing of glacial terminations was well simulated, but changes in CO_2 concentration lagged, and the amplitude of simulated changes were smaller than that indicated in the proxy record. In a later study using the same model Willeit et al., (2019) found that including regolith removal allowed them to better simulate Pleistocene climate variability, and increase the amplitude of the simulated variations. Whilst the results of these studies are impressive, EMICs have coarse resolution and many simplifications – particularly in the atmosphere compared to GCMs and Earth System Models (ESMs). The physical mechanisms, and climate feedbacks that can contribute to orbitally driven ice sheet growth and decay are still poorly understood and simulated in GCMs.

Our study is inspired by the findings of Erb et al. (2013) who quantified the role of radiative feedbacks to changes in obliquity. They found that a negative low cloud feedback, due

to a reduction in low cloud amount and cloud water content, impeded ice sheet initiation by opposing glaciation at times when orbital forcing would otherwise support it. A negative low cloud feedback has also been identified in other studies (Birch et al., 2017; Jochum et al., 2012) and highlights additional complications to understanding the orbit-climate relationship. Jochum et al., (2012) ran simulations using insolation from the last glacial inception (115 kya) and also found a reduction in low cloud amount, resulting in a negative shortwave (SW) cloud feedback. They calculated that the initial (orbital) forcing of 1.9 W m^2 above 60°N was amplified by the snow-ice-albedo feedback by 6.7 Wm^{-2} and was damped by a negative SW cloud feedback of 3.1 Wm^{-2}, due to a reduction in low cloud. Birch et al., (2017) used a high-resolution cloud resolving model to examine the role of clouds in glacial inception and their results confirmed those of Jochum et al (2012).

Clouds are one of the most challenging and uncertain aspects of the climate system (Boucher et al., 2013) and new research suggests that the negative feedback associated with cloud phase changes in existing models may be too strong (Tan et al., 2016). Cloud phase is poorly represented in global climate models, which have tended to underestimate the supercooled liquid fraction (SLF) in mixed phase clouds (MPCs) (Cesana et al., 2015; Komurcu et al., 2014). MPCs are common in the mid and high latitudes (Morrison et al., 2012; Shupe, 2011; Zhang et al., 2010) but are difficult to model for several reasons: there is a paucity of observational data (Illingworth et al., 2007; Morrison et al., 2012) and general difficulties in representing MPC microphysics (Komurcu et al., 2014; Lohmann & Hoose, 2009), in particular the conversion from liquid to ice known as the Wegner-Bergeron-Findeisen (WBF) process (Storelvmo et al., 2008; Tan & Storelvmo, 2016).

The cloud phase feedback can be explained as so: in response to warming the liquid-ice phase transition isotherm moves to higher altitudes such that, for a given altitude, the SLF is enhanced relative to the initial state. For a given amount of cloud water, supercooled liquid droplets are more reflective to SW radiation than cloud ice due to their smaller size and larger population (Murray et al., 2012; Pruppacher & Klett, 1978). The transition from ice to liquid therefore produces a negative feedback as supported by both models (Mitchell et al., 1989) and satellite observations (Tan et al., 2019). When SLFs are initially underestimated, this negative feedback is too strong and masks other cloud processes that generally yield positive feedbacks (Tan et al., 2016).

Using observationally constrained cloud phase, Tan et al., (2016) found that the liquid-to-ice transition isotherm moved upward, where there are fewer and thinner clouds, and poleward where incoming solar radiation is reduced. Subsequently the phase transition response to radiative perturbation is weakened and equilibrium climate sensitivity (ECS) increased. Climate sensitivity in the latest generation of climate models, the Coupled Modeling Intercomparison Project (CMIP6), has increased in the 27 models currently available (1.8 – 5.6 K) compared to previous estimates (1.5 – 4.5 K) (Bindoff et al., 2013). This is attributed to stronger positive cloud feedbacks (amount and scatter), and linked to reductions in low cloud cover and water content in the mid-latitudes in response to changes in sea-surface temperatures (SSTs) (Zelinka et al., 2020). The small negative feedback from low cloud scattering in CMIP5 is on average positive in CMIP6. This weaker liquid water path (LWP) increase with warming is qualitatively consistent with Tan et al., (2016) and several other studies (Bodas-Salcedo et al., 2019; Gettelman et al., 2019; McCoy et al., 2015; Zelinka et al., 2020).

159 This study examines the response of observationally constrained clouds to orbital forcing in
160 pairs of simulations in which obliquity is prescribed at the extremes of its Pleistocene range (Lo
161 and Hi simulations). We use the same model set up and observationally constrained SLF values
162 (SLF1 and SLF2) as used in Tan et al., (2016). However, in this work we explore the impact of
163 observationally constrained SLFs on the response to obliquity forcing rather than CO_2 forcing.
164 Changes in obliquity are not spatially uniform, with a larger impact in the higher latitudes than in
165 the tropics. Obliquity values are taken from the Erb et al., (2013) study which first evaluated
166 radiative feedbacks in response to orbital forcing and identified a negative high latitude cloud
167 feedback.

168

169 **2. Materials and Methods**

170 *2.1. Climate Model Setup*

171 The Community Earth System Model (CESM) version 1.0.6 (Hurrell et al., 2013) is
172 comprised of the atmospheric component CAM5.1 (Liu et al., 2012; Neale et al., 2010) which
173 has 30 vertical levels and uses the three-mode version of the Modal Aerosol Module (MAM3)
174 (Liu et al., 2012); the Community Land Model (CLM4.0) (Lawrence et al., 2011; Oleson et al.,
175 2010); the ocean model (Parallel Ocean Program Ocean model, POP2) (Smith et al., 2010) and
176 the Ice Model (Community Ice CodE, CICE4.0) (Holland et al., 2012; Hunke et al., 2010). In
177 these simulations CAM5.1 and CLM4.0 are run with a resolution of 1.9°x2.5° whilst POP2 and
178 CICE4.0 have a nominal 1° resolution. The DEF simulation is run with the default cloud
179 microphysics scheme (Morrison & Gettelman, 2008) and the standard ice-nucleation
180 parameterization scheme (Meyers et al., 1992) in which ice nucleating particle number
181 concentration is calculated based on temperature and supersaturation. For the SLF1 and SLF2

simulations the ice-nucleation parameterization scheme is updated (DeMott et al., 2015) to a more realistic scheme which enables ice nucleating particle number concentration to be diagnosed as a function of the concentration of large dust particles in addition to temperature. This allows for the spatial and temporal variability of dust ice nucleating particles (INP) to be taken into account. As in Tan et al., (2016) SLFs in SLF1 and SLF2 were determined from the results of a 256 member quasi Monte Carlo sampling approach in which six cloud microphysical parameters were modified, and the resulting cloud phase was compared with satellite data from NASA's Cloud-Aerosol-Lidar with Orthogonal Polarization (CALIOP) (Winker et al., 2009). The parameter combinations selected for SLF1 and SLF2 were very different (Table S1) but both produced SLFs in excellent agreement with CALIOP.

2.2. Climate Simulations

We use a pre-industrial model configuration (i.e. land mask, ice sheets, greenhouse gases, vegetation and aerosols) whereas Tan et al., (2016) used a present-day configuration. This leads to a large top-of-atmosphere (TOA) radiative imbalance which would require very long simulations to reduce. We re-tune the model slightly (Table S2) and the findings from our untuned simulations (not included) and tuned simulations are consistent.

Following Erb et al., 2013 we perform idealized simulations in which only obliquity is modified to a low (Lo) value of 22.079° and a high (Hi) value of 24.480° representative of the past 600 Kyr. DEF, SLF1 and SLF2 are run with Lo and Hi obliquity (six simulations) until the TOA energy budget is < 0.3 Wm^{-2} which takes between 350– 850 years for the different simulations (Table S3). These simulation lengths are long enough to capture broad changes in the atmosphere and surface ocean but are not long enough for the oceans to fully respond to the obliquity forcing. The final 50 years of the simulation are used as the input for cloud radiative

kernel computations, for calculations of climate means and for the International Satellite Cloud Climatology Project (ISCCP) satellite simulator analysis (Klein & Hartmann, 1993; Webb et al., 2001). The majority of results are presented as Lo-Hi anomalies as this convention reduces northern hemisphere (NH) summer insolation, which is conducive to a cooling climate and NH glaciation.

2.3. Downscaling Model

Because climate model resolutions are too coarse to capture the detail required for realistic ice sheet dynamics, i.e. underlying bedrock topography, (Birch et al., 2017; Pollard & Thompson, 1997), a downscaling approach was also used to determine the extent to which the differences in cloud parametrization would affect the persistence of snow cover in the low obliquity simulation. As in Notaro et al., (2014), the downscaling method we used employed the SNOW-17 snow accumulation and ablation model (Anderson 2006), which is used by the United States National Weather Service for real-time hydrologic modeling. SNOW-17 is driven by daily temperature and precipitation. Modern snow cover was simulated on a 1° by 1° latitude-longitude grid by using 30 years of observed daily temperature and precipitation from the data set compiled by Kluver et al., (2016). To simulate snow cover in the low obliquity experiments, the so-called "delta-change" approach is used (Lettenmaier et al., 1999). For each month, climatological differences in surface air temperature were computed between each low obliquity simulation and a corresponding historical simulation (using historical forcing from 1850-2000) with the same cloud parameterization. These differences were interpolated to the 1° by 1° grid and added to the 30-year observed daily temperature time series at each point. A similar approach was used for precipitation except that the ratio of low obliquity and historical

227 precipitation was determined, and the observed precipitation time series was multiplied by this
228 ratio.

229

230 **3. Results**

231 *3.1. Temperature and Insolation Seasonal Cycle*

232 Obliquity affects the annual latitudinal distribution of insolation and modulates
233 seasonality especially in the high latitudes. These changes have a negligible impact on global
234 annual mean insolation, with lower (Lo) obliquity reducing polar insolation in summer and
235 increasing it in winter. Figure 1 shows the annual mean Lo-Hi surface air temperature (SAT)
236 anomaly (colored contours) with the insolation anomaly overlaid (black contours). The negative
237 insolation anomaly (in all simulations) extends across almost all the northern hemisphere (NH)
238 from March to September. In the DEF experiment, negative SAT anomalies lag the insolation
239 anomaly by ~ 6 weeks and have a smaller spatial and temporal extent than the negative
240 anomalies in SLF1 and SLF2. In SLF1 and SLF2 negative SAT anomalies extend equator-wards
241 in March and over the entire NH (and globe) until January where a very small 0.25 K tropical
242 warming occurs.

243 Negative SAT anomalies in SLF1 and SLF2 extend into areas with a positive insolation
244 anomaly and indicate the importance of climate feedbacks over direct insolation forcing. The Lo-
245 Hi global annual mean SAT anomalies for our experiments are -0.79 K, -1.30 K and -1.36 K for
246 DEF, SLF1 and SLF2 respectively. This cooling signal and its extension to lower latitudes with
247 constrained SLF applies to both hemispheres, unlike other studies which simulate very little
248 cooling in the Southern Hemisphere (Jochum et al., 2012). These SAT anomalies indicate that

249 the climate response to obliquity forcing is considerably larger when cloud phase is
250 observationally constrained.

251 *3.2. Radiative Feedbacks*

252 We calculate the radiative feedbacks of surface albedo, atmospheric water vapor, vertical
253 temperature lapse rate and cloud optical properties using the radiative kernel method of climate
254 feedback analysis (Shell et al., 2008; Soden et al., 2008). Note that results are presented as the
255 effect of feedbacks on net TOA radiation ΔR_{net} (Wm^{-2}) and not as feedbacks ($Wm^{-2}\,K^{-1}$) as this
256 avoids dividing by small values of global mean ΔT (Erb et al., 2013). In the context of how our
257 results are presented: For Lo-Hi anomalies, a positive value of ΔR_{net} indicates a feedback effect
258 that opposes orbitally driven cooling. A negative value of ΔR_{net} indicates a feedback effect that
259 strengthens the orbital signal. Globally, the ΔR_{net} from all radiative feedbacks is ~1.6 to 1.7 times
260 stronger in SLF1 and SLF2 compared to DEF. Global mean ΔR_{net} from SW cloud and water
261 vapor feedbacks are much larger in SLF1 and SLF2 compared to DEF, whilst the ΔR_{net} from
262 lapse rate feedback is similar in all simulations and the ΔR_{net} from surface albedo feedback is
263 only marginally larger in SLF1 and SLF2. When broken down into hemispheres and regions
264 (Figure 2) the mid-latitude cloud feedback and tropical water vapor feedback effects stand out as
265 being much larger in SLF1 and SLF2 compared to DEF.

266 During late summer in the high latitude insolation is reduced due to low obliquity, which
267 should lead to local cooling. Over this period in DEF, column-integrated liquid (i.e. LWP)
268 reduces and acts to oppose and reduce cooling from this obliquity driven reduction in insolation
269 (Figure S1). In the SLF1 and SLF2 simulations this high-latitude LWP reduction in summer is
270 not evident, but a large increase in total (ice+liquid) water path (TWP) appears in the mid-

latitudes (30-60°N) which increases cloud reflectivity and thus cooling throughout the year (Figure S2).

In response to obliquity forcing (Lo-Hi), cooling leads to cloud liquid being converted to cloud ice, which is optically thinner. The cloud phase bias in DEF causes an exaggerated cloud thinning as too much liquid is converted to ice with cooling. This exaggerated reduction in cloud optical depth counters the other, mainly positive, cloud feedbacks and therefore weakens the spreading of high-latitude cooling to mid- and low latitudes. In contrast, the amplifying mid-latitude cloud feedback in SLF1 and SLF2 is twice as strong as in DEF, permitting high-latitude cooling to spread across the mid-latitudes towards the tropics. The slight cooling in the tropics (as opposed to the warming seen in DEF) is accompanied by a slight decrease in atmospheric water vapor, as expected according to the Clausius-Clapeyron relation. Since water vapor is a potent greenhouse gas, this reduction in water vapor increases outgoing longwave (LW) radiation and thus constitutes a powerful amplifying feedback in the tropics. High and mid-latitude cooling in DEF is not amplified by cloud feedbacks as in SLF1 and SLF2. This results in the slightly positive summer Lo-Hi tropical insolation anomaly producing a warming in DEF and thus a positive water vapor feedback that opposes high-latitude orbitally-forced cooling.

3.3. Decomposing the Cloud (Feedback) Response to Orbital Forcing

In order to more fully understand the changes in cloud properties that occur in response to orbital forcing we examine the output from the International Satellite Cloud Climatology Project satellite simulator (ISCCP) (Klein & Jakob, 1999; Webb et al., 2001) which is implemented in the atmosphere component of CESM, the Community Atmosphere Model (CAM5.1). The ISCCP simulator allows cloud properties in models to be diagnosed in a manner consistent with the satellite view from space. The radiative impact of changes in cloud amount (CLD), optical

294 depth (COT) and cloud top pressure (CTP) as well as a residual term are calculated following
295 Zelinka et al., (2012) and summarized by feedback in Figure 3 with the net feedback shown in
296 Figure S2. This de-composition of the net (SW+LW) cloud feedback into contributions from
297 CLD, CTP and COT reveals that the latter component is responsible for the difference in mid-
298 latitude cloud feedback between DEF on one hand, and SLF1 and SLF2 on the other. Because
299 the orbital signal is strongest between 60-90°N, it helps to consider this region first. Between 60-
300 90°N SW COT is positive in DEF whilst in SLF1 and SLF2 it is shifted to less positive values.
301 Between 30-60°N, SW COT has decreased from near zero in DEF, to -3 Wm^{-2} in SLF1 and
302 SLF2 across this latitude band. In the Southern Hemisphere, the SW COT feedback becomes
303 significantly less positive (60-90°S) and more negative (30-60°S) in SLF1 and SLF2 compared
304 to DEF.

305 *3.4. Glacial inception*

306 The central tenet of Milanković's orbital theory is that cooler summers allow high latitude snow
307 to survive the summer melt season. Perennial snow cover subsequently leads to snow-albedo
308 feedbacks, which amplify ice cap expansion and initiate the growth of large-scale ice-sheets.
309 Sediment cores indicate that in the NH the last glacial inception occurred ~ 115,000 years ago in
310 the region of Hudson Bay and Baffin Island over a period of around 20,000 years (Clark et al.,
311 1993). Furthermore, SLF2, which generally has a higher supercooled liquid water content than
312 SLF1 (Tan et al. 2016) exhibits more snow-free days than SLF1, in line with Tan & Storelvmo
313 2019, suggesting the importance of ice cloud microphysics on Arctic amplification. We gauge
314 the summer melt response to the cooling signal in these experiments by calculating the
315 percentage change in positive degree-days (PDD) for Lo-Hi over the June-July-August (JJA)
316 period (Figure 4a-c). PDD are calculated as the sum total of daily average temperatures above

0°C in a given time period. We focus on JJA as although Milanković theory considers caloric summer half year, the majority of glacial melt takes place over the short summer season. All three experiments show a substantial reduction in PDD (up to 50%) in the high Arctic, Hudson Bay area and over Baffin Island, which are likely locations of the last initiation of the Laurentide ice sheet. In SLF1 and SLF2 the reduction in PDD extends further into the mid-latitudes than DEF, in agreement with the increased extent of negative SATs.

As climate models are too coarse to capture the detail required for realistic ice sheet dynamics. we use a downscaling method to provide an additional metric for evaluating glacial inception. Figure 4d-e shows the average number of days without snow cover > 1" for the Lo - historical anomaly over the Canadian Arctic. SLF1 and SLF2 have fewer snow free days over the summer than DEF, with this increase in snow preservation occurring over the southern part of Baffin Island, eastwards of the Hudson Bay and over much of northern and middle Canada, which is in line with the proxy evidence (Clark et al., 1993). Because modern simulations were not available for this study, and the modern climate is warmer than the historical climate, our use of historical anomalies likely underestimates the duration of snow cover in the low obliquity experiments.

4. **Discussion and Conclusions**

We have repeated the experiments in Erb et al., (2013) to examine the obliquity driven climate response in a model with observationally constrained supercooled liquid fraction (SLF) in mixed phase clouds (MPCs). SLFs are increased in two experiments (SLF1 and SLF2) using a more realistic ice-nucleation scheme (DeMott et al., 2015) but using different methods in order to account for the uncertainties associated with MPC microphysics. These are compared with a default model (DEF) in which SLFs are known to be underestimated (Cesana et al., 2015;

Komurcu et al., 2014). Other studies have found that orbitally induced climate changes are opposed by negative high latitude low cloud feedbacks (Birch et al., 2017; Erb et al., 2013; Jochum et al., 2012). However, when realistic present-day SLFs are used, the strength of this negative cloud feedback is reduced which allows obliquity-driven cooling to spread to lower latitudes. This cooling leads to an increased liquid water path (LWP) and ice water path (IWP) in mid-latitude clouds and this positive cloud feedback further extends the cooling signal both throughout the year and leads to a strong tropical water vapor feedback.

We compare our three simulations with the CM2.1 the model used in the Erb et al., 2013 study. Overall the SAT response in CESM is larger than that in CM2.1: the response of SLF1 and SLF2 is 1.6-1.7 times that in DEF and is 2-3 times larger than that in CM2.1. The sum of net radiative feedbacks effects (ΔR_{net}) are 1.9 - 2.4 times larger in SLF1 and SLF2 compared with DEF and 2.6 – 3.5 times larger than in CM2.1. Reductions in positive degree days (PDDs) of up to 50% occur in the summer melt season in the Hudson Bay and Baffin Island area which have been identified as probable locations for the expansion of the Laurentide ice sheet (Clark et al., 1993). These and further reductions in PDD which extend into the mid-latitudes in SLF1 and SLF2, and reduction in snow-free days calculated from the downscaling approach provide further support that the climate in these experiments is more conducive to ice-sheet growth.

Column-integrated liquid (i.e. LWP) reduces and acts to oppose and reduce cooling from this obliquity driven reduction in insolation (Figure S1). This process is also seen in CM2.1. The cloud feedback processes that contribute to the extension and expansion of the cooling signal apply to both hemispheres (Figures 1, 3) unlike previous studies in which only a strong northern hemisphere cooling signal is simulated (Jochum et al., 2012). Southern hemisphere cooling is important for sea ice expansion in the Antarctic, which drives increased carbon

sequestration in the ocean. Proxy records indicate that early during the last glacial cycle around, 115 kya, polar cooling and sea ice expansion in the Antarctica were associated with an initial drawdown of CO_2 (35 ppm) (Kohfeld & Chase, 2017). In addition to the snowfall and ablation metrics which support larger ice sheet expansion in SLF1 and SLF2 than in DEF, increased southern hemisphere cooling and ice formation would sequester more CO_2.

Proxy reconstructions from the tropical oceans indicate that Pleistocene SSTs cooled prior to changes in continental ice volume (Dyez et al., 2016; Medina-Elizalde & Lea, 2005) and in regions SST changed in the opposite direction to changes in local annual insolation (Liu & Herbert, 2004). As ours is an idealized study, and we have only presented Lo-Hi surface temperature anomalies (Figure 1), subsequently explicit comparisons with proxy records are not suitable. However, in our work SLF1 and SLF2 both demonstrate tropical cooling throughout much of the year despite a positive insolation anomaly, whereas DEF and CM2.1 show a warming. This provides further support for the notion that high latitude cooling can drive tropical climate change, in qualitative agreement with proxy reconstructions.

Simulating cloud processes is a challenging area of study and it should be noted that the microphysics that contribute to high SLFs in mixed phase clouds are not completely understood: both reductions in the efficiency of the Wegner-Bergeron-Findeisen (WBF) process (Lohmann & Hoose, 2009; Storelvmo et al., 2008; Tan & Storelvmo, 2016) and the availability, size distribution and effectiveness of INPs such as mineral dust (Atkinson et al., 2013; Kok et al., 2017; Murray et al., 2012; Sagoo & Storelvmo, 2017) have a significant impact on SLFs and climate. The positive cloud and water vapor feedbacks which amplify the orbital signal in this work are unmasked because the high latitude negative low cloud feedback was not present in SLF1 and SLF2. Understanding the response of low Arctic clouds to changes in climate and sea-

ice cover is challenging (Kay et al., 2011; Kay & Gettelman, 2009) and thus the magnitude and even the presence of a high latitude summer low cloud feedback are still not well constrained. Finally, in summary, we find strong support for Milanković's orbital theory in this study when SLFs are observationally constrained. Enhanced cooling in the high latitudes leads to the unmasking of well-known positive mid-latitude cloud feedbacks and tropical water vapor feedback, which amplify the obliquity signal by additional cooling which reduces summer snow/ice melt.

Acknowledgments, Samples, and Data

- Simulations were run on the Yale High Performance Computing Cluster.
- Data availability: CESM model output relevant for study figures is available at https://doi.org/10.5281/zenodo.3891912
- The authors declare no competing interests.
- T.S. was supported by ERC grant 758005
- N.S was supported by NSF grant 1352417 whilst at Yale University

Author contributions

A.B conceived the project, A.B, T.S and N.S designed and organized this study. L.H, N.S, T.S, A.B carried out the analysis. J.D and B.R developed the downscaling software and made the calculations. L.H, N.S and T.S wrote the manuscript. All authors discussed and contributed to the manuscript.

References

Abe-Ouchi, A., Saito, F., Kawamura, K., Raymo, M. E., Okuno, J., Takahashi, K., & Blatter, H. (2013). Insolation-driven 100,000-year glacial cycles and hysteresis of ice-sheet volume. *Nature*, *500*(7461), 190–193.

Atkinson, J. D., Murray, B. J., Woodhouse, M. T., Whale, T. F., Baustian, K. J., Carslaw, K. S., et al. (2013). The importance of feldspar for ice nucleation by mineral dust in mixed-phase clouds. *Nature*, *498*(7454), 355–358.

Barnola, J.-M., Raynaud, D., Korotkevich, Y. S., & Lorius, C. (1987). Vostok ice core provides 160,000-year record of atmospheric CO2. *Nature*, *329*(6138), 408–414.

Bindoff, N. L., Stott, P. A., AchutaRao, K. M., Allen, M. R., Gillett, N., Gutzler, D., et al. (2013). Detection and attribution of climate change: from global to regional.

Birch, L., Cronin, T., & Tziperman, E. (2017). Glacial Inception on Baffin Island: The Role of Insolation, Meteorology, and Topography. *Journal of Climate*, *30*(11), 4047–4064. https://doi.org/10.1175/JCLI-D-16-0576.1

Bodas-Salcedo, A., Mulcahy, J. P., Andrews, T., Williams, K. D., Ringer, M. A., Field, P. R., & Elsaesser, G. S. (2019). Strong dependence of atmospheric feedbacks on mixed-phase microphysics and aerosol-cloud interactions in HadGEM3. *Journal of Advances in Modeling Earth Systems*, *11*(6), 1735–1758.

Boucher, O., Randall, D., Artaxo, P., Bretherton, C., Feingold, G., Forster, P., et al. (2013). Clouds and Aerosols: In Climate Change 2013: The Physical Science Basis Contribution of Working Group I to the Fifth Assessment Report of the Intergovernmental Panel on Climate Change. *K., Tignor, M., Allen, SK, Boschung, J., Nauels, A., Xia, Y., Bex, V., Midgley, PM, Eds*.

Cesana, G., Waliser, D. E., Jiang, X., & Li, J.-L. (2015). Multimodel evaluation of cloud phase transition using satellite and reanalysis data. *Journal of Geophysical Research: Atmospheres*, *120*(15), 7871–7892.

Clark, P. U., Clague, J. J., Curry, B. B., Dreimanis, A., Hicock, S. R., Miller, G. H., et al. (1993). Initiation and development of the Laurentide and Cordilleran ice sheets following the last interglaciation. *Quaternary Science Reviews*, *12*(2), 79–114.

Clark, P. U., & Pollard, D. (1998). Origin of the middle Pleistocene transition by ice sheet erosion of regolith. *Paleoceanography*, *13*(1), 1–9.

DeMott, P. J., Prenni, A. J., McMeeking, G. R., Sullivan, R. C., Petters, M. D., Tobo, Y., et al. (2015). Integrating laboratory and field data to quantify the immersion freezing ice nucleation activity of mineral dust particles. *Atmospheric Chemistry and Physics*, *15*(1), 393–409.

Dyez, K. A., Ravelo, A. C., & Mix, A. C. (2016). Evaluating drivers of Pleistocene eastern tropical Pacific sea surface temperature. *Paleoceanography*, *31*(8), 2015PA002873. https://doi.org/10.1002/2015PA002873

Erb, M. P., Broccoli, A. J., & Clement, A. C. (2013). The contribution of radiative feedbacks to orbitally driven climate change. *Journal of Climate*, *26*(16), 5897–5914.

Ganopolski, A., & Brovkin, V. (2017). Simulation of climate, ice sheets and CO2 evolution during the last four glacial cycles with an Earth system model of intermediate complexity. *Climate of the Past*, *13*, 1695–1716.

Gettelman, A., Hannay, C., Bacmeister, J. T., Neale, R. B., Pendergrass, A. G., Danabasoglu, G., et al. (2019). High climate sensitivity in the Community Earth System Model version 2 (CESM2). *Geophysical Research Letters*, *46*(14), 8329–8337.

454 Hays, J. D., Imbrie, J., Shackleton, N. J., & others. (1976). Variations in the Earth's orbit:
455 pacemaker of the ice ages. American Association for the Advancement of Science.
456 Retrieved from
457 https://www.researchgate.net/profile/J_Hays/publication/301325552_Variations_in_the_
458 Earth_pacemaker_of_the_ice_ages/links/573cca0c08ae9ace840fe240.pdf
459 Holland, M. M., Bailey, D. A., Briegleb, B. P., Light, B., & Hunke, E. (2012). Improved sea ice
460 shortwave radiation physics in CCSM4: the impact of melt ponds and aerosols on Arctic
461 sea ice*. *Journal of Climate*, *25*(5), 1413–1430.
462 Hunke, E. C., Lipscomb, W. H., Turner, A. K., & others. (2010). CICE: the Los Alamos Sea Ice
463 Model Documentation and Software User's Manual Version 4.1 LA-CC-06-012. *T-3*
464 *Fluid Dynamics Group, Los Alamos National Laboratory*, *675*. Retrieved from
465 http://oceans11.lanl.gov/svn/CICE/tags/release-5.1/doc/cicedoc.pdf
466 Hurrell, J. W., Holland, M. M., Gent, P. R., Ghan, S., Kay, J. E., Kushner, P. J., et al. (2013).
467 The community earth system model: a framework for collaborative research. *Bulletin of*
468 *the American Meteorological Society*, *94*(9), 1339–1360.
469 Huybers, P. (2006). Early Pleistocene glacial cycles and the integrated summer insolation
470 forcing. *Science*, *313*(5786), 508–511.
471 Huybers, P. (2011). Combined obliquity and precession pacing of late Pleistocene deglaciations.
472 *Nature*, *480*(7376), 229–232.
473 Illingworth, A. J., Hogan, R. J., O'connor, E. J., Bouniol, D., Delanoë, J., Pelon, J., et al. (2007).
474 Cloudnet: Continuous evaluation of cloud profiles in seven operational models using
475 ground-based observations. *Bulletin of the American Meteorological Society*, *88*(6), 883–
476 898.

Jochum, M., Jahn, A., Peacock, S., Bailey, D. A., Fasullo, J. T., Kay, J., et al. (2012). True to Milankovitch: Glacial inception in the new community climate system model. *Journal of Climate*, *25*(7), 2226–2239.

Kay, J. E., & Gettelman, A. (2009). Cloud influence on and response to seasonal Arctic sea ice loss. *Journal of Geophysical Research: Atmospheres*, *114*(D18), D18204. https://doi.org/10.1029/2009JD011773

Kay, J. E., Holland, M. M., & Jahn, A. (2011). Inter-annual to multi-decadal Arctic sea ice extent trends in a warming world. *Geophysical Research Letters*, *38*(15), L15708. https://doi.org/10.1029/2011GL048008

Klein, S. A., & Hartmann, D. L. (1993). The Seasonal Cycle of Low Stratiform Clouds. *Journal of Climate*, *6*(8), 1587–1606. https://doi.org/10.1175/1520-0442(1993)006<1587:TSCOLS>2.0.CO;2

Klein, S. A., & Jakob, C. (1999). Validation and sensitivities of frontal clouds simulated by the ECMWF model. *Monthly Weather Review*, *127*(10), 2514–2531.

Kluver, D., Mote, T., Leathers, D., Henderson, G. R., Chan, W., & Robinson, D. A. (2016). Creation and validation of a comprehensive 1 by 1 daily gridded North American dataset for 1900–2009: Snowfall. *Journal of Atmospheric and Oceanic Technology*, *33*(5), 857–871.

Kohfeld, K. E., & Chase, Z. (2017). Temporal evolution of mechanisms controlling ocean carbon uptake during the last glacial cycle. *Earth and Planetary Science Letters*, *472*, 206–215.

Kok, J. F., Ridley, D. A., Zhou, Q., Miller, R. L., Zhao, C., Heald, C. L., et al. (2017). Smaller desert dust cooling effect estimated from analysis of dust size and abundance. *Nature Geoscience*, *10*(4), 274–278. https://doi.org/10.1038/ngeo2912

Komurcu, M., Storelvmo, T., Tan, I., Lohmann, U., Yun, Y., Penner, J. E., et al. (2014). Intercomparison of the cloud water phase among global climate models. *Journal of Geophysical Research: Atmospheres*, *119*(6), 2013JD021119. https://doi.org/10.1002/2013JD021119

Lambert, F., Delmonte, B., Petit, J.-R., Bigler, M., Kaufmann, P. R., Hutterli, M. A., et al. (2008). Dust-climate couplings over the past 800,000 years from the EPICA Dome C ice core. *Nature*, *452*(7187), 616–619.

Lawrence, D. M., Oleson, K. W., Flanner, M. G., Thornton, P. E., Swenson, S. C., Lawrence, P. J., et al. (2011). Parameterization improvements and functional and structural advances in Version 4 of the Community Land Model. *Journal of Advances in Modeling Earth Systems*, *3*(1), M03001. https://doi.org/10.1029/2011MS00045

Lettenmaier, D. P., Wood, A. W., Palmer, R. N., Wood, E. F., & Stakhiv, E. Z. (1999). Water resources implications of global warming: A US regional perspective. *Climatic Change*, *43*(3), 537–579.

Liautaud, P. R., Hodell, D. A., & Huybers, P. J. (2020). Detection of significant climatic precession variability in early Pleistocene glacial cycles. *Earth and Planetary Science Letters*, *536*, 116137.

Lisiecki, L. E. (2010). Links between eccentricity forcing and the 100,000-year glacial cycle. *Nature Geoscience*, *3*(5), 349–352.

Lisiecki, L. E., & Raymo, M. E. (2005). A Pliocene-Pleistocene stack of 57 globally distributed benthic δ18O records. *Paleoceanography*, *20*(1). Retrieved from http://onlinelibrary.wiley.com/doi/10.1029/2004PA001071/full

Liu, X., Easter, R. C., Ghan, S. J., Zaveri, R., Rasch, P., Shi, X., et al. (2012). Toward a minimal representation of aerosols in climate models: Description and evaluation in the Community Atmosphere Model CAM5. *Geoscientific Model Development*, *5*(3), 709.

Liu, Z., & Herbert, T. D. (2004). High-latitude influence on the eastern equatorial Pacific climate in the early Pleistocene epoch. *Nature*, *427*(6976), 720–723.

Lohmann, U., & Hoose, C. (2009). Sensitivity studies of different aerosol indirect effects in mixed-phase clouds. *Atmospheric Chemistry and Physics*, *9*(22), 8917–8934.

Mantsis, D. F., Clement, A. C., Broccoli, A. J., & Erb, M. P. (2011). Climate feedbacks in response to changes in obliquity. *Journal of Climate*, *24*(11), 2830–2845.

Martínez-Garcia, A., Rosell-Melé, A., Jaccard, S. L., Geibert, W., Sigman, D. M., & Haug, G. H. (2011). Southern Ocean dust-climate coupling over the past four million years. *Nature*, *476*(7360), 312–315.

McCoy, D. T., Hartmann, D. L., Zelinka, M. D., Ceppi, P., & Grosvenor, D. P. (2015). Mixed-phase cloud physics and Southern Ocean cloud feedback in climate models. *Journal of Geophysical Research: Atmospheres*, *120*(18), 9539–9554.

Medina-Elizalde, M., & Lea, D. W. (2005). The mid-Pleistocene transition in the tropical Pacific. *Science*, *310*(5750), 1009–1012.

Meyers, M. P., DeMott, P. J., & Cotton, W. R. (1992). New primary ice-nucleation parameterizations in an explicit cloud model. *Journal of Applied Meteorology*, *31*(7), 708–721.

Milanković, M. (1941). *Kanon der Erdbestrahlung und seine Anwendung auf das Eiszeitenproblem*. na.

544 Mitchell, J. F., Senior, C. A., & Ingram, W. J. (1989). C02 and climate: a missing feedback?
545 *Nature*, *341*(6238), 132–134.
546 Morrison, H., & Gettelman, A. (2008). A New Two-Moment Bulk Stratiform Cloud
547 Microphysics Scheme in the Community Atmosphere Model, Version 3 (CAM3). Part I:
548 Description and Numerical Tests. *Journal of Climate*, *21*(15), 3642–3659.
549 https://doi.org/10.1175/2008JCLI2105.1
550 Morrison, H., de Boer, G., Feingold, G., Harrington, J., Shupe, M. D., & Sulia, K. (2012).
551 Resilience of persistent Arctic mixed-phase clouds. *Nature Geoscience*, *5*(1), 11–17.
552 https://doi.org/10.1038/ngeo1332
553 Murray, B. J., O'Sullivan, D., Atkinson, J. D., & Webb, M. E. (2012). Ice nucleation by particles
554 immersed in supercooled cloud droplets. *Chemical Society Reviews*, *41*(19), 6519–6554.
555 Neale, R. B., Chen, C.-C., Gettelman, A., Lauritzen, P. H., Park, S., Williamson, D. L., et al.
556 (2010). Description of the NCAR community atmosphere model (CAM 5.0). *NCAR*
557 *Tech. Note NCAR/TN-486+ STR*. Retrieved from
558 https://www.ccsm.ucar.edu/models/ccsm4.0/cam/docs/description/cam4_desc.pdf
559 Notaro, M., Lorenz, D., Hoving, C., & Schummer, M. (2014). Twenty-first-century projections
560 of snowfall and winter severity across central-eastern North America. *Journal of Climate*,
561 *27*(17), 6526–6550.
562 Oleson, K. W., Lawrence, D. M., Gordon, B., Flanner, M. G., Kluzek, E., Peter, J., et al. (2010).
563 Technical description of version 4.0 of the Community Land Model (CLM). Retrieved
564 from http://citeseerx.ist.psu.edu/viewdoc/summary?doi=10.1.1.172.7769

565 Petit, J.-R., Mourner, L., Jouzel, J., Korotkevich, Y. S., Kotlyakov, V. I., & Lorius, C. (1990).
566 Palaeoclimatological and chronological implications of the Vostok core dust record.
567 Retrieved from http://www.nature.com/nature/journal/v343/n6253/abs/343056a0.html
568 Pollard, D., & Thompson, S. L. (1997). Driving a high-resolution dynamic ice-sheet model with
569 GCM climate: ice-sheet initiation at 116 000 BP. *Annals of Glaciology*, *25*, 296–304.
570 Pruppacher, H. R., & Klett, J. D. (1978). Microphysics ofclouds andprecipitation. *Reidel,*
571 *Dordrecht, Holland, 714pp*.
572 Raymo, M. E., Lisiecki, L. E., & Nisancioglu, K. H. (2006). Plio-Pleistocene Ice Volume,
573 Antarctic Climate, and the Global δ18O Record. *Science*, *313*(5786), 492–495.
574 https://doi.org/10.1126/science.1123296
575 Raymo, M. E., & Nisancioglu, K. H. (2003). The 41 kyr world: Milankovitch's other unsolved
576 mystery. *Paleoceanography*, *18*(1).
577 Rind, D., Peteet, D., & Kukla, G. (1989). Can Milankovitch orbital variations initiate the growth
578 of ice sheets in a general circulation model? *Journal of Geophysical Research:*
579 *Atmospheres*, *94*(D10), 12851–12871.
580 Sagoo, N., & Storelvmo, T. (2017). Testing the sensitivity of past climates to the indirect effects
581 of dust. *Geophysical Research Letters*, *44*(11), 2017GL072584.
582 https://doi.org/10.1002/2017GL072584
583 Saltzman, B., Hansen, A. R., & Maasch, K. A. (1984). The late Quaternary glaciations as the
584 response of a three-component feedback system to Earth-orbital forcing. *Journal of the*
585 *Atmospheric Sciences*, *41*(23), 3380–3389.

586 Shell, K. M., Kiehl, J. T., & Shields, C. A. (2008). Using the radiative kernel technique to
587 calculate climate feedbacks in NCAR's Community Atmospheric Model. *Journal of*
588 *Climate*, *21*(10), 2269–2282.
589 Shupe, M. D. (2011). Clouds at Arctic atmospheric observatories. Part II: Thermodynamic phase
590 characteristics. *Journal of Applied Meteorology and Climatology*, *50*(3), 645–661.
591 Sigman, D. M., & Boyle, E. A. (2000). Glacial/interglacial variations in atmospheric carbon
592 dioxide. *Nature*, *407*(6806), 859–869.
593 Smith, R., Jones, P., Briegleb, B., Bryan, F., Danabasoglu, G., Dennis, J., et al. (2010). The
594 parallel ocean program (POP) reference manual ocean component of the community
595 climate system model (CCSM) and community earth system model (CESM). *Rep. LAUR-*
596 *01853*, *141*, 1–140.
597 Soden, B. J., Held, I. M., Colman, R., Shell, K. M., Kiehl, J. T., & Shields, C. A. (2008).
598 Quantifying climate feedbacks using radiative kernels. *Journal of Climate*, *21*(14), 3504–
599 3520.
600 Storelvmo, T., Kristjánsson, J. E., Lohmann, U., Iversen, T., Kirkev\a ag, A., & Seland, Ø.
601 (2008). Modeling of the Wegener–Bergeron–Findeisen process—implications for aerosol
602 indirect effects. *Environmental Research Letters*, *3*(4), 045001.
603 Tabor, C. R., & Poulsen, C. J. (2016). Simulating the mid-Pleistocene transition through regolith
604 removal. *Earth and Planetary Science Letters*, *434*, 231–240.
605 Tabor, C. R., Poulsen, C. J., & Pollard, D. (2015). How obliquity cycles powered early
606 Pleistocene global ice-volume variability. *Geophysical Research Letters*, *42*(6), 1871–
607 1879.

608 Tan, I., & Storelvmo, T. (2016). Sensitivity study on the influence of cloud microphysical
609 parameters on mixed-phase cloud thermodynamic phase partitioning in CAM5. *Journal*
610 *of the Atmospheric Sciences*, *73*(2), 709–728.
611 Tan, I., Storelvmo, T., & Zelinka, M. D. (2016). Observational constraints on mixed-phase
612 clouds imply higher climate sensitivity. *Science*, *352*(6282), 224–227.
613 Tan, I., Oreopoulos, L., & Cho, N. (2019). The Role of Thermodynamic Phase Shifts in Cloud
614 Optical Depth Variations With Temperature. *Geophysical Research Letters*, *46*(8), 4502–
615 4511.
616 Webb, M., Senior, C., Bony, S., & Morcrette, J.-J. (2001). Combining ERBE and ISCCP data to
617 assess clouds in the Hadley Centre, ECMWF and LMD atmospheric climate models.
618 *Climate Dynamics*, *17*(12), 905–922.
619 Westerhold, T., Marwan, N., Drury, A. J., Liebrand, D., Agnini, C., Anagnostou, E., et al.
620 (2020). An astronomically dated record of Earth's climate and its predictability over the
621 last 66 million years. *Science*, *369*(6509), 1383–1387.
622 Willeit, M., Ganopolski, A., Calov, R., & Brovkin, V. (2019). Mid-Pleistocene transition in
623 glacial cycles explained by declining CO2 and regolith removal. *Science Advances*, *5*(4),
624 eaav7337.
625 Winker, D. M., Vaughan, M. A., Omar, A., Hu, Y., Powell, K. A., Liu, Z., et al. (2009).
626 Overview of the CALIPSO mission and CALIOP data processing algorithms. *Journal of*
627 *Atmospheric and Oceanic Technology*, *26*(11), 2310–2323.
628 Zachos, J., Pagani, M., Sloan, L., Thomas, E., & Billups, K. (2001). Trends, Rhythms, and
629 Aberrations in Global Climate 65 Ma to Present. *Science*, *292*(5517), 686–693.
630 https://doi.org/10.1126/science.1059412

631 Zelinka, M. D., Klein, S. A., & Hartmann, D. L. (2012). Computing and partitioning cloud
632 feedbacks using cloud property histograms. Part I: Cloud radiative kernels. *Journal of*
633 *Climate*, *25*(11), 3715–3735.
634 Zelinka, M. D., Myers, T. A., McCoy, D. T., Po-Chedley, S., Caldwell, P. M., Ceppi, P., et al.
635 (2020). Causes of higher climate sensitivity in CMIP6 models. *Geophysical Research*
636 *Letters*, *47*(1), e2019GL085782.
637 Zhang, D., Wang, Z., & Liu, D. (2010). A global view of midlevel liquid-layer topped stratiform
638 cloud distribution and phase partition from CALIPSO and CloudSat measurements.
639 *Journal of Geophysical Research: Atmospheres*, *115*(D4).

640
641

642 **Figure Captions**

643 **Figure 1**. Seasonal changes in zonally averaged surface air temperature (SAT) and insolation
644 shown as Lo-Hi obliquity anomalies. a) DEF, b) SLF1 and c) SLF2. SAT is shown in color
645 shading with the global annual mean SAT anomaly value shown at the top of each figure in
646 parenthesis. Overlaid black contours and labels denote the Lo-Hi surface insolation anomaly
647 with the thick black line indicating the zero-insolation contour.

648 **Figure 2**. The effect of radiative feedbacks partitioned into individual components (surface
649 albedo, lapse rate, water vapor, cloud shortwave (SW), cloud longwave (LW) and residuals (SW
650 and LW)) and split by region and hemisphere: a) & b) Northern and Southern hemisphere mean
651 (NH & SH); c) & d) tropics (0-20°N and 0-20°S; e) & f)) mid-latitudes (30-60°N and 30-60°S)
652 and g) & h) high latitudes (60-90°N and 60-90°S). Note that results are presented as the effect of
653 feedbacks on net TOA radiation (Wm^{-2}) and not as surface temperature-mediated feedbacks
654 (Wm^{-2} K^{-1}).

655 **Figure 3**. Longwave (LW) and shortwave (SW) and net cloud feedback effects (expressed as
656 ΔRnet in Wm^{-2}) calculated using the International Satellite Cloud Climatology Project satellite
657 simulator (ISCCP). LW feedbacks are shown in the top row: a) DEF, b) SLF1, c) SLF2, SW
658 feedbacks are shown in the bottom row: d) DEF, e) SLF1 and f) SLF2 with feedbacks due to
659 changes in cloud amount (CLD) shown in orange, cloud optical depth (COT) in green, cloud top
660 pressure (CTP) in blue, a residual component in magenta and total feedbacks are shown in black.

661 **Figure 4**. Indicators of change in summer (June, July, August) snow preservation. Percentage
662 change in positive-degree days (PDD) polewards of 30°N for northern hemisphere for Lo-Hi
663 anomaly shown for a) DEF, b) SLF1 and c) SLF2 Lo-Hi experiments with blue indicating fewer
664 PDD and increased likelihood of snow preservation. A downscaling model was used to calculate
665 the average number of days without snow $\geq$ 1" in the Canadian Arctic for the Lo-Pre-industrial
666 anomaly for DEF, SLF1 and SLF2. The anomaly of d) SLF1-DEF and e) SLF2-DEF are shown
667 in the bottom row where blue indicates an increase in snow covered days.

668

Figure 1.

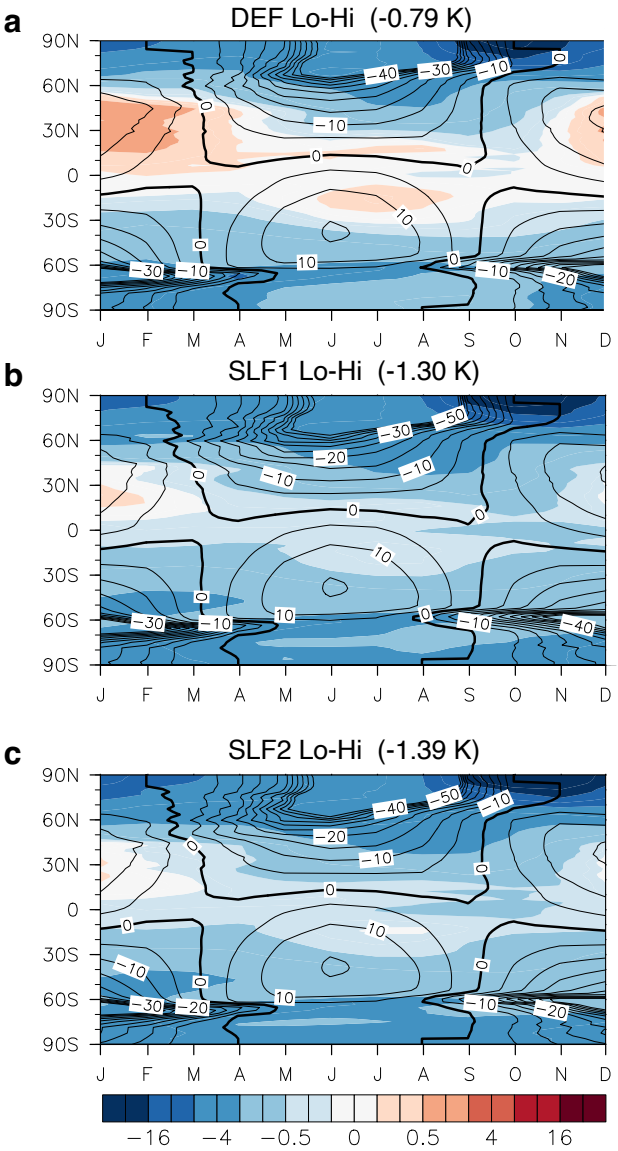
a
DEF Lo-Hi (-0.79 K)
b
SLF1 Lo-Hi (-1.30 K)
c
SLF2 Lo-Hi (-1.39 K)
90N
60N
30N
0
30S
60S
90S
J F M A M J J A S O N D
−16 −4 −0.5 0 0.5 4 16

Figure 2.

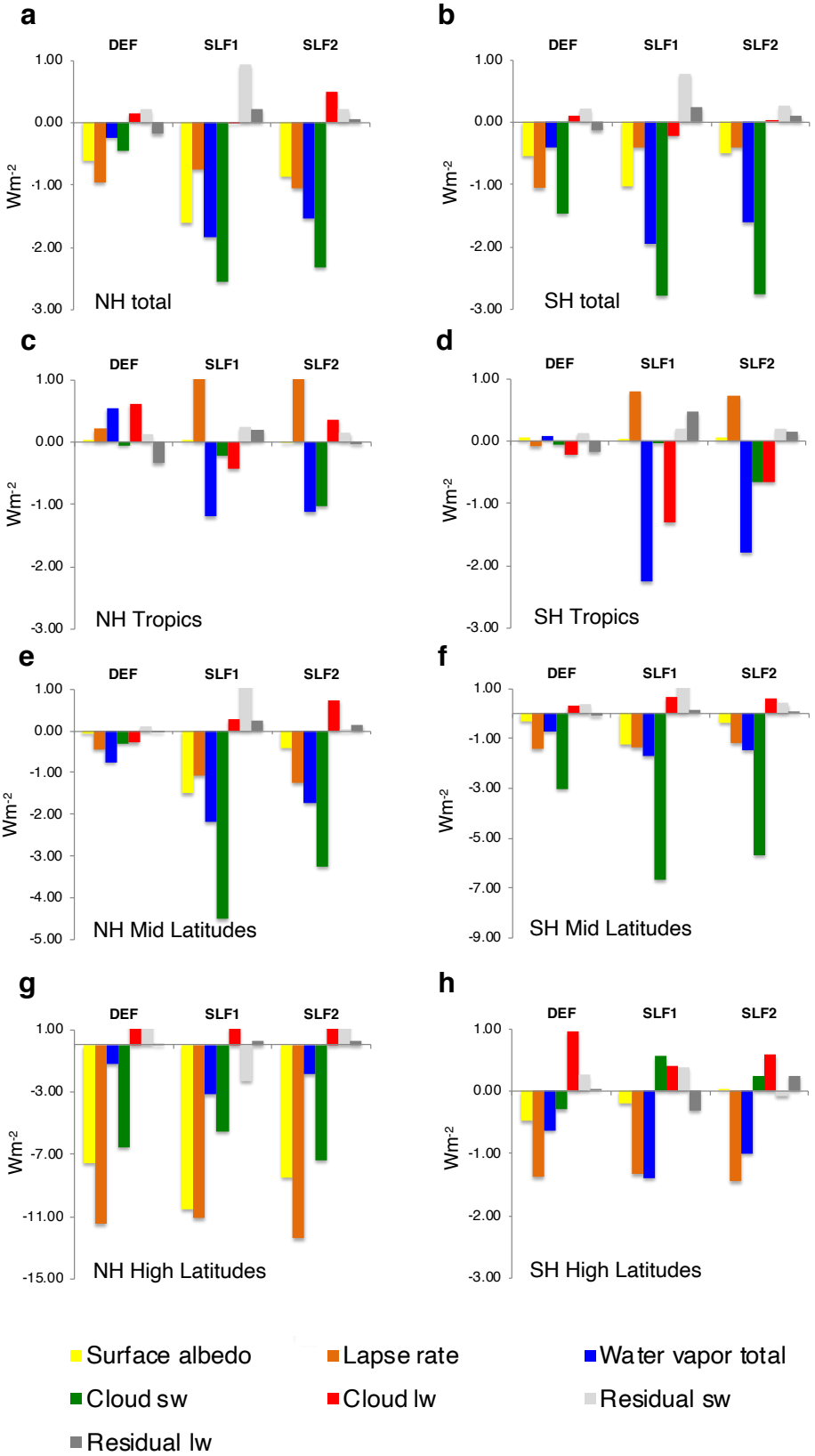
a
DEF
SLF1
SLF2
1.00
0.00
-1.00
-2.00
-3.00
Wm-2
NH total
b
DEF
SLF1
SLF2
1.00
0.00
-1.00
-2.00
-3.00
Wm-2
SH total
c
DEF
SLF1
SLF2
1.00
0.00
-1.00
-2.00
-3.00
Wm-2
NH Tropics
d
DEF
SLF1
SLF2
1.00
0.00
-1.00
-2.00
-3.00
Wm-2
SH Tropics
e
DEF
SLF1
SLF2
1.00
0.00
-1.00
-2.00
-3.00
-4.00
-5.00
Wm-2
NH Mid Latitudes
f
DEF
SLF1
SLF2
1.00
-1.00
-3.00
-5.00
-7.00
-9.00
Wm-2
SH Mid Latitudes
g
DEF
SLF1
SLF2
1.00
-3.00
-7.00
-11.00
-15.00
Wm-2
NH High Latitudes
h
DEF
SLF1
SLF2
1.00
0.00
-1.00
-2.00
-3.00
Wm-2
SH High Latitudes
Surface albedo
Lapse rate
Water vapor total
Cloud sw
Cloud lw
Residual sw
Residual lw

Figure 3.

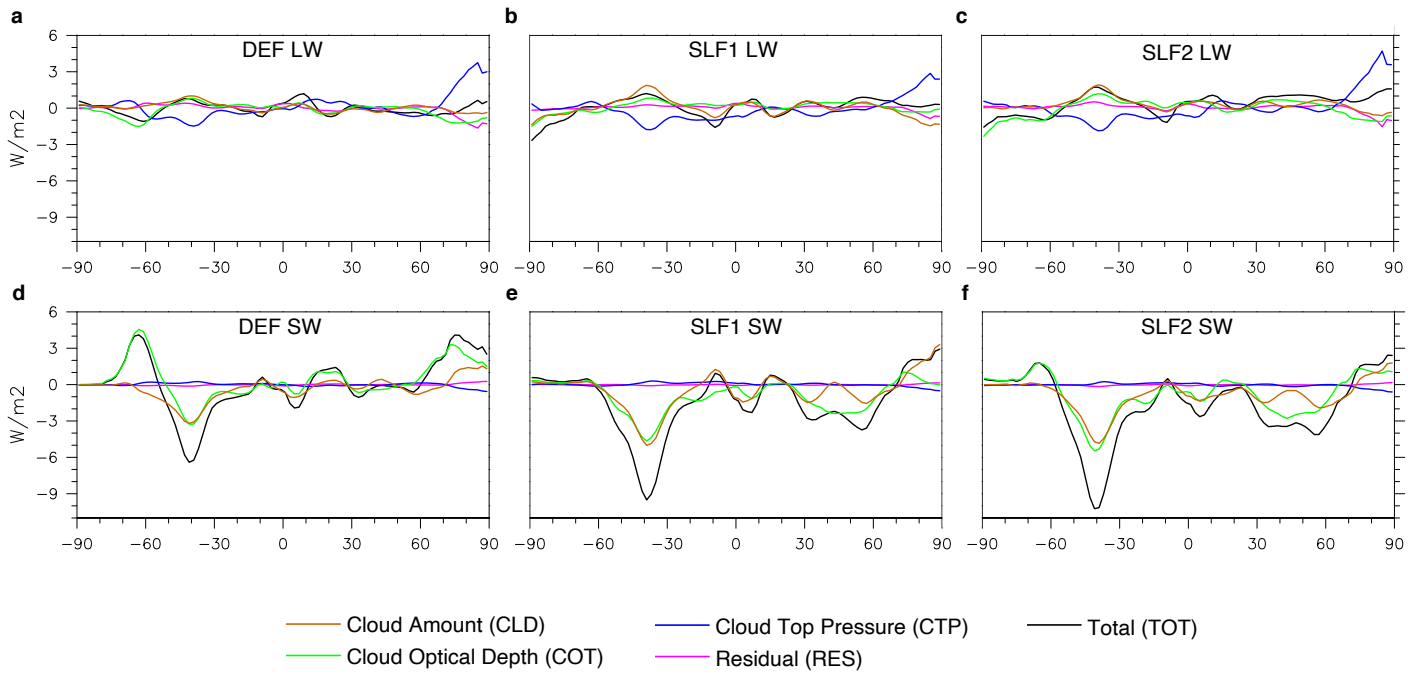
a
DEF LW
b
SLF1 LW
c
SLF2 LW
d
DEF SW
e
SLF1 SW
f
SLF2 SW
W/m2
6
3
0
−3
−6
−9
−90
−60
−30
0
30
60
90
Cloud Amount (CLD)
Cloud Optical Depth (COT)
Cloud Top Pressure (CTP)
Residual (RES)
Total (TOT)

Figure 4.

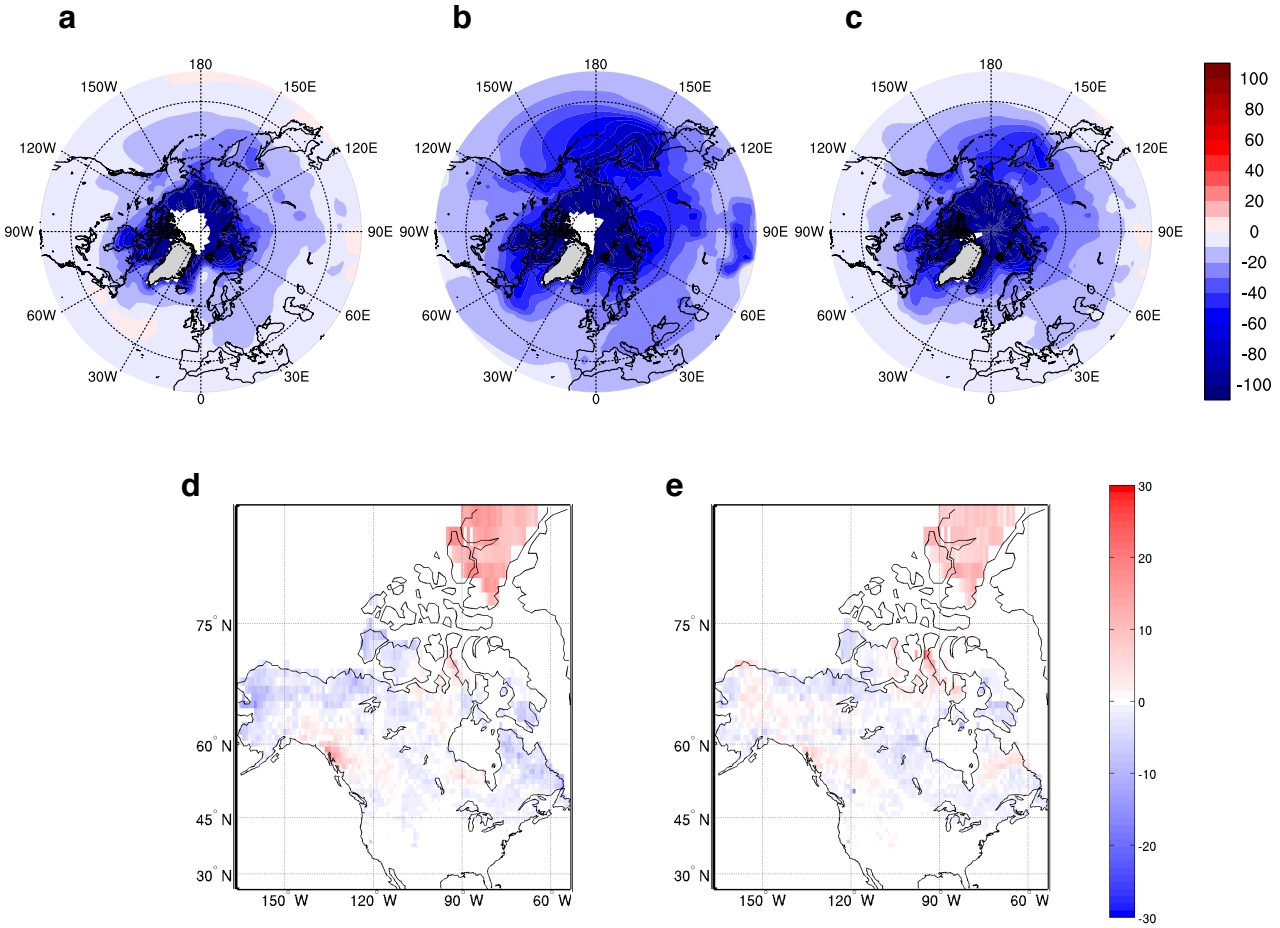
a
b
c
180
150W
150E
120W
120E
90W
90E
60W
60E
30W
30E
0
100
80
60
40
20
0
-20
-40
-60
-80
-100
d
e
75° N
60° N
45° N
30° N
150° W
120° W
90° W
60° W
30
20
10
0
-10
-20
-30